Biogeosciences Discuss., 9, 18755–18798, 2012
www.biogeosciences-discuss.net/9/18755/2012/
doi:10.5194/bgd-9-18755-2012

Biogeosciences Discussions

Physical transport properties of marine microplastic pollution

A. Ballent, A. Purser, P. de Jesus Mendes, S. Pando, and L. Thomsen

OceanLab, Jacobs University, 28759 Bremen, Germany

Received: 24 November 2012 – Accepted: 30 November 2012
– Published: 19 December 2012

Correspondence to: A. Ballent (a.ballent@jacobs-alumni.de)

Published by Copernicus Publications on behalf of the European Geosciences Union.

Abstract

Given the complexity of quantitative collection, knowledge of the distribution of microplastic pollution in many regions of the world ocean is patchy, both spatially and temporally, especially for the subsurface environment. However, with knowledge of typical hydrodynamic behavior of waste plastic material, models predicting the dispersal of pelagic and benthic plastics from land sources into the ocean are possible. Here we investigate three aspects of plastic distribution and transport in European waters. Firstly, we assess patterns in the distribution of plastics found in fluvial strandlines of the North Sea and how distribution may be related to flow velocities and distance from source. Second, we model transport of non-buoyant preproduction pellets in the Nazaré Canyon of Portugal using the MOHID system after assessing the density, settling velocity, critical and depositional shear stress characteristics of such waste plastics. Thirdly, we investigate the effect of surface turbulences and high pressures on a range of marine plastic debris categories (various densities, degradation states and shapes tested) in an experimental water column simulator tank and pressure laboratory. Plastics deposited on North Sea strandlines varied greatly spatially, as a function of material composition and distance from source. Model outputs indicated that such dense production pellets are likely transported up and down canyon as a function of tidal forces, with only very minor net down canyon movement. Behaviour of plastic fragments under turbulence varied greatly, with the dimensions of the material, as well as density, playing major determining roles. Pressure was shown to affect hydrodynamic behaviours of only low density foam plastics at pressures $\geq$ 60 bar.

1 Introduction

Microplastic pollution is ubiquitous in marine environments. Rivers and storm drains can carry material from inland sources to the ocean (Moore et al., 2011). From coastal areas plastics can reach the sea via wind action, and material can be directly released

to the ocean by illegal dumping, or from shipping and recreational activities (Derraik, 2002). Plastics, often in the form of pre-production pellets, filaments, film, foam, or larger consumer products may be physically degraded and fragmented by wave action, UV radiation exposure and biofouling (Andrady, 2011; Moore et al., 2011). Plastic material is transported throughout the oceans by currents, tides, shear stresses, and other oceanic processes, but the majority of material is found concentrated in neustonic and coastal environments (Cole et al., 2011).

Consumer plastic densities range from ~ 0.9–$1.4\,g\,mL^{-1}$ (Morét-Ferguson et al., 2010). Plastics of lower density (LD) than seawater ($\sim 1.03\,g\,mL^{-1}$; Morét-Ferguson et al., 2010) are found predominantly within the surface layer of the oceans, and in highest concentrations in subtropical gyres (Moore et al., 2001; Martinez et al., 2009; Law et al., 2010). Material of higher density than seawater (HD) is concentrated in marine and fluvial benthic environments (Galgani et al., 2000; Claessens et al., 2011; Costa et al., 2011; Mordecai et al., 2011). Plastics of both density categories can be found in coastal areas (Lattin, 2004; Barnes et al., 2009; Browne et al., 2010). Due to the cost and low efficiency of collecting microplastics via sediment trap, trawl, Autonomous Underwater Vehicle collection (AUVs), diving, remote camera deployment or beach combing (Barnes et al., 2009; Ryan et al., 2009), data on microplastic abundance across the global marine environment is very limited and does not reflect the full likely distribution of such materials, either spatially or temporally.

We conducted a series of empirical quantitative and qualitative experiments to investigate how oceanic forces may influence the physical transport of microplastics, in three distinguishable marine environments. Our three research aims were as follows: (1) to sample and quantify coastal strandline plastics at four sites along the Weser and Elbe Rivers in Northern Germany, (2) to model transport of benthic microplastic pellets in a submarine canyon and (3) to explore the effects of turbulence and pressure on the vertical distribution of neustonic microplastics.

1.1 Strandline plastics

Studies on coastal microplastics in Hawaii, the Mediterranean Sea, Brazil, Belgium, and the UK show that plastic debris is not evenly distributed even on small spatial scales (McDermid and McMullin, 2004; Browne et al., 2010; Costa et al., 2010; Turner and Holmes, 2011; Claessens et al., 2011). For example, microplastic counts at four beach collection sites on Midway Atoll varied between 10 and 17 645 pieces total (McDermid and McMullin, 2004). To contribute to the growing worldwide data collection of coastal microplastics, samples were collected, sorted, sized and quantified from four sites in Northern Germany.

1.2 Modelling transport of benthic microplastics

High density (HD) microplastics are commonly found on beaches, in river sediments, on continental shelf slopes and in deep sea benthic environments (Cole et al., 2011). They compose approximately half of all manufactured plastics (USEPA, 1992; Morét-Ferguson et al., 2010). Although growing interest in the situation has driven a number of recent studies, data of plastic pollution in the deep-sea is scarce, mainly due to the difficulties of deep-sea sampling (Claessens et al., 2011). One extensive study covering European shelf areas reported spatial densities of 0.064–2.63 plastic pieces (≥ 2 cm diameter) per hectare (Galgani et al., 2000). On the California continental shelf, benthic trawls (net mesh size 333 microns) in the 20 cm above the seafloor at 30 m depth collected microplastics in spatial densities of 6.5 and 1.5 pieces m^{-3} before and after a storm, respectively (Lattin et al., 2004). Before the storm, plastic density at the seafloor was roughly 60 times the plastic density at the ocean surface (< 1 piece m^{-3}). Recently, in a study supported by the HERMIONE programme, Remotely Operated Vehicle (ROV) video surveys of benthic marine litter in the submarine canyons off the coast of Portugal reported highest abundances in canyon heads located off the coast of populated cities (Mordecai et al., 2011).

In this study, rather than rely on field observations to determine debris abundance and distribution, we attempt to predict how high density plastics may be transported throughout a submarine canyon ecosystem, by determining the physical transport properties of collected preproduction pellets in the laboratory and applying these results in a hydrodynamic model.

1.3 Factors influencing vertical transport of neustonic microplastics

Low density (LD) plastic accumulates in the neustonic zones of the worlds' sub-tropical gyres at spatial densities up to hundreds of thousands of pieces per square kilometer (Moore et al., 2001; Martinez et al., 2009; Law et al., 2010; Andrady, 2011; Cole et al., 2011). The concentrations of plastic found in the underlying mixed layer, and how meteorological and oceanographic conditions may influence these concentrations, are not well known (Doyle et al., 2011). Field studies indicate a general trend between higher wind speed and lower surface plastic counts, suggesting that surface plastics can be drawn down vertically into the water column (Lattin et al., 2004; Thompson et al., 2004; Ryan et al., 2009; Proskurowski et al., 2010; Doyle et al., 2011; Kukulka et al., 2012); however, the temporal and spatial extent over which this occurs is not well understood. In this study, two qualitative laboratory experiments were conducted to determine the effect of turbulence on the vertical distribution of various types of LD plastics (fragments, foams, filaments, films and pellets) from the samples collected at the Weser and Elbe Rivers (see Sect. 2.1) and how increasing pressure (depth) may impact on the buoyancy of LD and HD plastics.

2 Methods

2.1 Strandline plastics of Weser and Elbe Rivers

Plastic fragments were collected from two strandline sample stations on both the Elbe River (Hamburg) and Weser River (Harriersand Island), where buoyant natural and

anthropogenic debris is stranded after a high tide. The top 10–15 cm of flotsam was collected from a 1 m^2 area at each of the four sites, after which plastics were manually sorted from the flotsam using tweezers. Plastic debris from each of these sources was sorted into five categories (film, fragment, mono-filament, preproduction pellet (primary microplastic granule) and foam) and stored in petri dishes. The particles' area, Feret's diameter (or filament length) and minimum Feret's diameter were quantified and measured using the *ImageJ* (v. 1.45 s) (Rasband, 1997–2012) software application "analyze particles" tool on photographs with color threshold applied (Fig. 1). In *ImageJ* the Feret's diameter is defined as the "maximum distance between two points on the selection boundary" (Ferreira and Rasband, 2011, p. 123).

2.2 Modelling transports of benthic microplastics

A number of experimental tests were carried out to determine the characteristics and settling behaviour of three categories of HD plastics. A large sample of collected preproduction pellets from the beaches of Los Angeles County, California was received from the Algalita Marine Research Foundation for use in this study. Samples of black, opaque and transparent pre-production pellets were used in these tests. The spatial dimensions of the pellets were assessed using *ImageJ* (Rasband, 1997–2012), as described in Sect. 2.1.

2.2.1 Density

The average density of the pellets of each category was determined by measuring the weight of a random subsample of pellets and the water displacement of the subsample using distilled water and a graduated cylinder. Density calculations were repeated with 5 subsample sets for each pellet category.

2.2.2 Settling rates

Settling velocities of the three pellet categories were determined by filming particles sinking through a 1 m still saltwater column (salinity 36 psu). We subtracted JPG images 1 s apart from the video stream, and used the *ImageJ* software (Rasband, 1997–2012) to determine settling speed after the method described in Pabortsava et al. (2011). The experimental run included ~ 50 HD black pellets, ~ 80 HD opaque pellets and ~ 50 HD transparent pellets.

2.2.3 Deposition and resuspension velocity determination

A 20 cm erosion microcosm similar to that described by Tolhurst et al. (2000) simulates benthic shear environments, and was used to determine the flow velocities at which bedload, resuspension, and deposition of the three categories of pellets occur. Runs were conducted with two groups of pellets: ~ 300 HD black pellets, ~ 200 HD opaque/transparent pellets (4 repetitions each) according to a predefined calibration table (Gust, unpublished data) relating rotor angular speed, pump flow and the resultant flow velocity (U^*). Using the water density, the shear velocity values were converted to shear stress values, [N m^{-2}], giving τ_b, τ_{cr} and τ_d (See Appendix A). The experiments were run in a stepwise manner, in which the bottom shear was manually increased over seven, 2-min long steps (Table 1) using a controlling unit to adjust the rotational speed of a plastic disk inside the chamber and an adjustable flow meter attached to the pump discharge tubing (Tolhurst et al., 2000). Experiments were filmed to allow for better analysis of particle behavior in laminar flows. The bedload shear velocity U^*_b was defined as the shear velocity at which 50 % of the particles rolled, slid or saltated on the chamber floor (percentages determined by direct observation and video analysis). The critical erosion velocity, U^*_{cr}, was defined as the shear velocity when 75 % of the particles were suspended in the water column. U^*_d, the depositional shear velocity was defined as the flow velocity at which all pellets had settled from suspension.

2.2.4 Hydrodynamic model transport simulation

Using empirical size, density, settling velocity, critical and depositional shear stress data of the HD black pellets, the MOHID hydrodynamic model (www.mohid.com) generated pellet transport predictions for the Nazaré Canyon, Portugal. Modelled particle trajectories for plastic pellets ($n = 2004$ per box) originating in four 0.5 m^3 "monitor boxes" (depths 59 m, 262 m, 331 m and 2657 m) within the Nazaré Canyon, were plotted for a 56 day period. Accurate atmospheric and oceanographic data for the time period between 15 March and 20 May 2009 was available to drive the physical parameters of the model. The numerical model was adapted for the HD black pellet data from one used previously in the modelling of organo-mineral aggregate transport, as given in Pando et al. (2011). Monitor box 1 was located in the canyon head, Box 4 toward the bottom of the canyon and Boxes 2 and 3 placed between these points within the canyon (Fig. 2).

2.3 Factors influencing vertical transport of neustonic microplastics

2.3.1 Effect of turbulence

Under standard conditions, turbulence dissipation rates (ε) at the surface boundary layer and thermocline range between 10^{-3}–10^{-1} W m^{-3} (Sanford, 1997; Petersen et al., 2009). In the stratified interior of the open ocean ε is commonly ~ 10^{-7} W m^{-3} (Petersen et al., 2009). To reproduce these turbulence intensities in a controlled environment, a Multiscale Experimental Ecosystem Research Center pelagic/benthic (MEERC P/B) type C tank as developed by Crawford and Sanford (2001) was used. The cylindrical 1 m^3 tank is fitted with horizontally rotating paddles (Fig. 3a) capable of replicating turbulence intensities of the dimension and structure shown in Fig. 3b (Sanford, 1997; Crawford and Sanford, 2001; Stiansen and Sundby, 2001; Petersen et al., 2009; Porter et al., 2010). The average turbulence intensity within the tank is directly related to the rotation speed of the paddles (Fig. 4 and Table 2; see Appendix B). Seven types of LD plastic were tested: LD pellets (LA Beach, $\rho \sim 0.709$ g cm^{-3}), films, foam,

mono-filament, and fragments of three size classes (≥ 10 mm, 5–10 mm and ≤ 5 mm). The largest fragment category (LD fragment, LA beach, $\rho \sim 0.698\,\mathrm{g\,cm^{-3}}$) consisted of irregular but ∼ 3 mm thick flattened pieces all of the same plastic composition. The medium and small fragments and remaining subsamples were collected from the Elbe and Weser sites (see Sect. 2.1) and varied in shape, size and type (Table 3).

To study how the buoyancy force of the plastics and the turbulent forces of the water interacted, the turbulence intensity within the water column was increased step-wise, with each step consisting of a minimum of 4 right-left cycles (5 forward rotations and 5 backward rotations), starting at 3 RPM and increasing to 27 RPM in increments of 3 RPM, turbulence dissipation rates ε ranging from 1.58×10^{-4} to $2.21\,\mathrm{W\,m^{-3}}$.

2.3.2 Effect of hydrostatic pressure

A pressure laboratory was used to observe the effect of increasing pressure on the buoyancy of microplastic debris. Direct visual observation was achieved using a digital camera in a 200 bar-proof Plexiglas pressure housing (Meerestechnik Bremen GmbH) inside a pressure laboratory. The plastics were kept in a saltwater (36 psu) environment using a 10 cm diameter Plexiglas cylindrical container with a rubber sealed lid and rubber bladder suspended within the pressure chamber. A manual hydraulic pump was used to slowly increase the pressure from 1 to 200 bar over 20 min and a valve released the pressure again. Sub-samples of HD opaque pellets, HD transparent pellets, HD fragments, LD fragments, LD pellets, and foams (both clean and biofilmed from Elbe Site 2) were tested.

3 Results

3.1 Strandline plastics of Weser and Elbe Rivers

The Elbe strandline contained the largest number of plastic pieces, mostly fragments and foams. Histograms of the samples depict the size and type distributions (Fig. 5).

When comparing the urban Elbe sites to the rural Weser sites consistently higher counts are found in urban areas; ∼ 5000–7000 pieces $\mathrm{m^{-3}}$ and ∼ 150–700 pieces $\mathrm{m^{-3}}$, respectively as extrapolated from sample counts. Pellets were most consistently abundant across sites, whereas films were almost exclusively found at Elbe Site 1. Fragments, pellets and foams were the three types of plastic found at each site. As determined from the measured Feret's diameter, pieces smaller than 5 mm were most abundant, followed by pieces between 5 and 10 mm and then pieces 10–15 mm. Table 3 lists size and count data for all samples according to piece type. The area and minimum Feret's diameter of filaments were not measured.

3.2 Modelling transports of benthic microplastics

3.2.1 Laboratory experimentation

The LA beach sample consisted of preproduction pellets and fragments of both high and low density which could be divided into six groups: HD black pellets with homogenous appearance, HD opaque pellets, HD transparent pellets, LD translucent pellets containing small entrapped bubbles, HD fragments and LD fragments. The average Feret's diameter of the pellets was 4.8 mm, while the flattened fragments of the LA beach sample measured ∼ 12.7 mm.

The density of the pellets ranged across values above and below the density of sea water ($1.03\,\mathrm{g\,cm^{-3}}$); black, opaque and transparent pellets were roughly 10 % more dense than sea water whereas the buoyant translucent pellets were about 20 % less dense (Table 4). The velocity at which the HD pellets from the LA Beach site settled varied from 20–60 $\mathrm{mm\,s^{-1}}$ (Table 5). The settling velocities of the black and opaque pellets varied little between individual pellets. There appeared to be two distinct groups of transparent pellets however, with settling velocities ∼ 35 $\mathrm{mm\,s^{-1}}$ and ∼ 70 $\mathrm{mm\,s^{-1}}$. Pellets with higher density in most cases had faster settling velocities; this was not the case for HD opaque pellets.

The two groups of pellets used in the resuspension chamber investigations behaved as expected given their densities and settling velocities. Black pellets began bedload transport in the first time-step (1.4×10^{-2} N m^{-2}) and almost all pieces were in rolling or saltating motion before any pellets were suspended. Critical erosional shear stress was determined to be ~ 0.14 N m^{-2}. At the highest possible shear stress achieved in the chamber (~ 0.2 N m^{-2}) almost all black pellets were in suspension (Fig. 6a). In contrast, the majority of the opaque/transparent group was *not* significantly suspended at the highest shear stress. In general, this group showed more resistance to erosion and less uniform behavior; opaque pellets eroded most easily and transparent pellets least. Approximately 85 % of all pellets were transported by saltation (nearing critical erosion threshold) at a shear stress of 0.2 N m^{-2} (Fig. 6b) and the last pieces settled at $\sim 4.6 \times 10^{-2}$ N m^{-2}. All shear stress values in Table 6 are approximated from direct observation and video analysis and are averaged across replicates.

Accuracy of the erosion experiment is low due to reliance on observation to determine the exact stage during the time-step experiment when the pellets alter their behavior. Pellets had a slow response time to changes in flow velocity and did not behave uniformly within or between replicates, possibly due to slight differences in particle properties (i.e. shape, size, density, degree of bio-fouling). It was also often difficult to determine whether a pellet was in suspension or bedload transport, and therefore define the shear stress threshold separating the two behaviors. Additionally, the pump had a large influence on the instantaneous shear within the chamber and the resulting transport behavior of the pellets. The pump flow fluctuated slightly on high frequencies and between replicate runs, sometimes causing suspended pellets to fall back to bedload transport due to an abrupt loss in pumping power. The restricted power of the pump also limited the maximum shear stress generated in the chamber. Despite these obstacles in determining exact shear stress values, the particles generally behaved consistently across repeated runs, allowing critical velocity and shear stress values to be approximated to the closest half-step.

3.2.2 Transport modelling

In the Nazaré Canyon simulation model, HD black pellets showed little displacement from the monitor boxes. Three output parameters were used to characterize the pellet transport behavior: distance (the total distance a pellet travelled [km]), displacement (the net distance a pellet was transported [km]), and velocity [km yr^{-1}]. As depicted in Fig. 7, averages for each parameter were calculated twice for each box; once for (a) all pellets ($n = 2004$) and once for (b) those pellets which were transported out of the monitor box during the model simulation period (1 pellet from Box 1, 13 pellets from Box 2, 53 pellets from Box 3 and 39 pellets from Box 4). In general, pellets traveled greater distances than they were displaced, indicating the pellets were transported in an oscillating manner, up and down canyon repeatedly. The average transport distances for all pellets was around 0.1 km, with an average displacement of 0.04 km. Average velocities ranged from 0.1 to 0.9 km yr^{-1}; however, the maximum velocity of an escaped pellet was 7.03 km yr^{-1}. Pellets in Monitor box 1 were transported the least distance while pellets from Monitor box 2 were, on average, displaced the furthest. Pellets from Monitor box 4 traveled on average the largest distances (in oscillatory up and down canyon motion).

The residence time of the HD black pellets in each monitor box is depicted in Fig. 8 as the fraction of pellets over time. The number of pellets in Box 1 fluctuates slightly in a sinusoidal manner around 100 % of initial number of pellets for the entirety of the model simulation period in a manner suggestive of a tidal rhythm. In Boxes 2, 3 and 4 tracer fractions change in a similar pattern, although to a lesser degree, but also change abruptly at certain points of time, indicating forces additional to tides act upon the pellets' transport at greater depths. These events occur simultaneously in each of the three deepest boxes signifying that the pellets' movements are forced by a large scale event, not small scale disturbances. In Box 2, 97 % of particles still remained inside the box at the end of the model simulation period, whereas in Boxes 3 and 4, approximately 66 % of pellets remained. Residence time can also be calculated using

the number of escaped particles and the model run-time as

$$T = \frac{\text{particles}}{\Delta\text{particles} \cdot \text{days}^{-1}} \quad , \tag{1}$$

which gives 315, 24, 6 and 8 yr for pellets in Monitor boxes 1–4, respectively.

3.3 Factors influencing vertical transport of neustonic microplastics

3.3.1 Turbulence assay

Studying the random nature of turbulent flows required a qualitative approach and heavy reliance on observation. Figure 9 shows the percentage of pieces, as determined by observation, of each plastic type submerged at each step of increasing turbulence intensity. Turbulence dissipation rate, ε, is plotted to show increasing turbulence levels associated with increasing wind shear. Overall, plastic composition (density) appeared to have the largest influence on vertical displacement, followed by size and flatness. Large, irregularly shaped pieces (e.g. films and filaments) were most susceptible to turbulence and were drawn below the surface at the lowest turbulence intensities of 2.5 cm s^{-1}. The plastics most resistant to surface turbulence were the round LD pellets. The paddle rotation often generated visible vortices extending from the surface and dissipating within 1–5 s of formation. Some of these were forceful enough to pull large, buoyant pieces below the surface, where they would disperse within the water column before returning to the surface. Pieces with irregular shape or densities close to that of the seawater were often submerged by small scale turbulence invisible to the observer.

LD pellets submerged to maximum 20 cm depth during the formation and dissipation of vortices at the fastest rotation speed (27 RPM). At lower turbulence intensities, pellets would occasionally submerge 1–2 cm before popping back to the surface. LD fragments 10–15 mm in size were observed separately from those < 10 mm. Similar to

the case of LD pellets, only ∼ 10 % of large fragments were submerged at the highest turbulence dissipation rates ($\varepsilon = 2.2$ W m^{-3}). The smallest fragments were affected at much lower turbulence intensities; approximately 70–80 % remained submerged for longer than 1 min at turbulence intensities (U_{RMS}) of 7.0 cm s^{-1}. Foams behaved similarly to LD pellets; both plastic types would occasionally become slightly submerged with strong vortex events at turbulence intensities of 5.5 cm s^{-1} or greater. Films and filaments were most susceptible to turbulence, several pieces submerging during the third rotation step (9 RPM) where turbulence intensities within the chamber averaged at ∼ 2.5 cm s^{-1}, and almost all pieces submerged before the final rotation step (27 RPM; $U_{\text{RMS}} \sim 7.0$ cm s^{-1}). The film and filament pieces with the most irregular shape were more readily submerged than thick, rigid, or flat pieces, though interestingly, flatness had a two-sided effect. Flat pieces of plastic had higher resistance to submerging (likely due to larger area affected by surface tension) but once within the water column they remained below the surface longer due to a slower rising speed and susceptibility to turbulences. In general, microplastics which were submerged at lower turbulence intensities also remained within the water column for longer time periods than those less easily submerged. Some fragments, films and filaments remained submerged for the duration of the experiment only returning slowly to the surface (at rates ∼ 0.1–0.003 m s^{-1}) after paddle rotation was stopped and flow velocities significantly reduced.

When the turbulence dissipation rates produced in the MEERC p/b water column simulation tank are correlated to wind speed, the effect of increased wind shear on surface counts of various debris types can be visualized. Equation (2), taken from MacKenzie and Leggett (1993) relates wind speed, W [m s^{-1}] to approximate turbulence dissipation rate, ε [W m^3] at a certain depth (here $z = 0.5$ m)

$$W = \sqrt[3]{\frac{\varepsilon \cdot z}{5.82 \cdot 10^{-6}}} \, . \tag{2}$$

Table 2 shows how average turbulence dissipation levels generated in the water column simulator can be related to wind speeds over the ocean surface.

3.3.2 Pressure assay

The only plastics affected by pressures ≤ 200 bar were some partially degraded/biofilm covered Styrofoam pieces (Fig. 10a–d). The most biofilm rich pieces began to sink at 60 bar corresponding to 600 m depth, and four relatively large (> 10 mm), less degraded pieces lost buoyancy at pressures of 140, 150, 170 and 180 bar, sinking slowly to the bottom of the chamber. When pressure was slowly released pieces regained buoyancy; however, when removed from the chamber, most pieces remained partially compressed. The least degraded/biofilm covered pieces were the least compressed. In a second and third run, subsamples of LD fragments and HD opaque/transparent pellets (Fig. 10e, f) and LD pellets (Fig. 10g, h) were tested, with no visible pressure effects apparent. The buoyancies of these microplastics were not affected by an increase in pressure up to 200 bar.

4 Discussion

4.1 Strandline plastics

Plastic quantities and types found in near-shore marine environments depend on the size and distance of plastic sources. The Elbe sites, located near the city center of Hamburg, contained significantly higher concentrations of debris than the Weser sites located on the outskirts of Bremen. This can be explained by assuming that more debris was released into the environment from the more densely populated city of Hamburg than from the smaller city of Bremen. Similar findings have been reported by Galgani et al. (1996) in a study of benthic macro-debris in the Gulf of Lions in the Mediterranean Sea, where larger accumulations of debris occurred in the submarine canyons off the cities of Nice and Marseille, and by Browne et al. (2010) who studied microplastics in sediments of the Tamar Estuary in the UK. However, another explanation is that much debris from inland sources is deposited within the strandline and sediment of riverbanks

and estuaries before it reaches the marine environment with the result that smaller quantities of debris are found along a river with increasing distance from the source (Browne et al., 2010). Findings from Galgani et al. (1996), Browne et al. (2010), Costa et al. (2011) and Mordecai et al. (2011) suggest that debris is transported similarly to sediment, and may become buried in sedimentation events. Browne et al. (2010) also suggest that in areas of low flow velocity, wind forces potentially push buoyant plastics and other flotsam to the riverbank where it can be deposited.

The type of sediment and flotsam on the bank may affect the degree to which debris is "filtered" from the water. For example, rocky shores should have a lower capacity to retard microplastic transport but may more effectively remove larger debris from the water. A general trend between the size of organic material and the size of microplastics was observed (data not shown). The Elbe strandline contained much smaller sized debris than the Weser strandline. Wood chips, degrading leaf pieces, small twigs and seeds made up the majority of the Elbe material, whereas that found at the Weser strandline comprised primarily of large reeds and drift wood. This compositional difference is another possible explanation of why larger counts of microplastics were found at the Elbe than Weser sites.

Current and tidal flow velocities may also affect the removal rates of plastics from river and coastal waters. Strong currents would have a higher eroding capacity for high density debris, transporting such material down-current or to areas of slower flow velocity. Flow velocities and sediment loads correlate well with debris transport capacities of rivers (Galgani et al., 2000). Moreover, rivers and estuaries in regions of strong tidal variation or large water level fluctuations may deposit greater amounts of microplastics due to the frequent occurrence of low flow velocities and the regular occurrence of high tides. Similarly, areas with greatly reduced flow velocity, estuaries, deltas, bays and harbors accumulate more debris as compared to high discharge river plumes where debris is more easily dispersed (Galgani et al., 1996, 2000; Browne et al., 2010; Claessens et al., 2011). Benthic and coastal topography (e.g. ripples or indentations in the sediment, canyons, slopes, bioturbation mounds, rocks etc.) which affect local

flow velocities, pressure gradients and inhibit flow may also influence whether or not microplastic pieces are deposited or eroded.

4.2 Modelling transports of benthic microplastics

The Nazaré Canyon model reveals that HD black pellets are dispersed extremely slowly and only 0.05–2.6 % of pellets escape within a 56 day period from their original location. Pellets near shore were transported regularly by tidal forces but were not dispersed. Sudden displacement events occurred more frequently at depth; possibly as a result of increased turbulence following storms, breaking internal waves, canyon turbidity flows, etc. Considering that the majority of plastic waste comes from land (Cole et al., 2011), this data may indicate that the majority of small HD plastics remain in coastal areas. This is supported by Mordecai et al. (2011) who found a correlation between macro debris in the Lisbon and Setubal submarine canyons off Portugal and distance from the coastline. The model results also suggest that debris which is displaced from the coast becomes well dispersed within the shelf, slope and abyssal ecosystems, potentially sparing them from high exposures, but intensifying consequences for more shallow regions. However, this does not mean that benthic debris may not accumulate in certain zones where further transport is inhibited by benthic topography as reported by Galgani et al. (1996) and Mordecai et al. (2011). Models could be used to locate and identify these areas from high resolution physical oceanography and topography data. For higher accuracy, additional local field data (e.g. particle counts from box core sediment samples and near bottom sediment trap samples) should be used with such models.

Critical erosion values in this model were determined in a laminar flow environment by simulating the logarithmic benthic boundary layer velocities found in deep sea environments (Thomsen et al., 2002). However, turbulent flows generated by tides, waves and uneven bottom surfaces also play a role in the resuspension of benthic particles. Using both laminar- and turbulence-induced critical erosion shears would improve future models. The pelagic-benthic water column simulation tanks used in the turbulence

experiments (see Sect. 3.1.1.) can also accurately mimic turbulence-induced benthic shears (Crawford and Sanford, 2001). When modelling benthic microplastic transport in various locations it must be considered that critical erosion shear values for microplastics and the forces required for resuspension may vary between shallow coastal areas and the deep seafloor. Wave action, tidal flows and the depth of the mixed layer may well have greater influence in shallow areas, with bottom currents, turbidity flows and storm events of greater significance in deeper areas.

In Table 7, a comparison between the HD black pellets from this study and similarly sized organo-mineral aggregates of the Iberian continental margin studied by Thomsen et al. (2002) is made for average diameter (d_{50}), density, settling velocity and critical shear stress. In Fig. 11, the difference is illustrated by plotting each of these on the quartz erosion curve as taken from Thomsen et al. (2002). The pellets have a relatively high settling velocity and erosional shear stresses approximately 5 times greater than 4 mm aggregates; overall, they behave more similarly to large sand particles or gravel than benthic boundary layer aggregates of similar size.

4.3 Factors influencing vertical transport of neustonic microplastics

The vertical transport of buoyant microplastics may be as important as horizontal transport when determining the extent of debris in regions of the ocean and consequences for marine ecosystems. For example, microplastics which reside, even temporarily, within the water column may be consumed by pelagic organisms, not only those feeding at the surface.

The turbulence assay was used to simulate wind shear- and wave- generated turbulence within the upper meter of the open ocean (MacKenzie and Leggett, 1993) with the aim of correlating wind speeds with the percentage of each investigated plastic type vertically displaced. Wind is a good proxy for estimating turbulence intensities of the upper mixed layer (MacKenzie and Leggett, 1993); however, comparing laboratory turbulence levels to those found in natural systems is difficult due to scale differences and methods of turbulence generation. In natural systems vertical displacement may

be restricted by the depth of the mixed layer, or extended by strong downwelling between Langmuir circulation cells. The laboratory experiments are simplified and only represent the turbulence dissipation component as a sum of factors which may affect vertical distribution of plastics; they do not directly simulate natural sources of surface turbulence (e.g. waves, bubbles and wind shear). Nevertheless, the laboratory generated ε values (1.5×10^{-4}–$2.2\,\mathrm{W\,m^{-3}}$) corresponded reasonably well with ε values found in the upper ocean surface layer (10^{-3}–$10^{-1}\,\mathrm{W\,m^{-3}}$) (Sanford, 1997; Petersen et al., 2009) and observations were compatible with field observations of trends relating surface trawl counts and wind speed (Law et al., 2010; Kukulka et al., 2012). For example, Moore et al. (2001) reported that subsurface trawls in the North Pacific gyre contained mostly biofilmed filament type plastics, which were also the most readily submerged in the turbulence assay of this study.

At the ocean surface, turbulence intensities decrease rapidly with depth (MacKenzie and Leggett, 1993); thus, turbulence intensities within the simulation tank could be used to imitate a certain depth within the mixed layer. From this point of view, further studies may reveal insights into how much time a particular particle remains below the surface under particular wind conditions and how quickly the vertical distribution of neustonic plastic adjusts to changes in wind speed.

The pressure assay demonstrates the potential for very low density plastics to be trapped at greater depths within the ocean basins in the event that it is brought to those depths via e.g. a sinking animal carcass which had ingested the plastics while alive. While this is not a likely sink pathway for large quantities of plastics it may present unknown consequences to abyssal ecosystems.

5 Conclusions

This investigation was an attempt to gauge the degree to which the intrinsic properties of plastic debris fragments affect their transport within the marine environment. From these results, it can be clearly seen that the density, shape and size of a piece

of plastic influence its transport, in addition to the external forcing parameters such as seawater density, seabed topography, flow velocity, turbulence, and pressure. It is crucial to understand how microplastics are transported to effectively estimate their global distribution, residence times, convergence zones and ecological consequences using hydrodynamic models. The model runs presented here indicated the slow transport of benthic microplastic in the Nazaré Canyon, which suggests an intensified long term exposure to plastics for those benthic ecosystems. Future research should focus on the ecological consequences of such exposures, particularly in critical areas such as biodiversity hotspots, to allow the development of preventative measures and policy/legislation changes if required. Decreasing the amount of plastic debris originating from urban consumers would greatly reduce exposure levels in many deep sea regions close to shore, such as the Atlantic canyon ecosystems focused on in the current study.

Vertical transport of microplastics leads to questions such as (1) to what degree is plastic ingestion by plankton facilitated by the increased encounter rates resulting from turbulence and mixing (Doyle et al., 2011) and (2) how may this affect the rate of persistent organic pollutants (POPs) entering food chain. Further research is needed to be able to more accurately estimate the amount of plastic residing in the oceans and to better understand the behavior of the smallest microplastics and their sinks within the natural environment.

Further investigation of the physical transport properties of marine microplastic pollution should include the use of models simulating a variety of benthic environments and should incorporate improved simulation techniques of wind induced turbulence, the effect of surface tension on neustonic plastics, how size affects the degree of consequence and risk for organisms and how pressures greater than 200 bar affect plastic buoyancy.

Appendix A

Relating shear velocity to shear stress

$$\tau = (U^*)^2 \times \rho \quad \text{(A1)}$$

τ [N m^{-2}] is shear stress, U^* [m s^{-1}] is shear velocity, and ρ [kg m^{-3}] is the density of seawater (Thomsen et al., 2002).

Appendix B

Relating paddle rotation to turbulence intensity in water column simulation tank

The mean turbulence intensity (root mean square velocity with the mean not removed),

$$U_{\mathrm{RMS}} = \sqrt{\frac{1}{3}[\langle (U+u)^2\rangle + \langle (V+v)^2\rangle + \langle (W+w)^2\rangle)]} \quad [\mathrm{cm\,s^{-1}}] \quad \text{(B1)}$$

and the mean turbulent dissipation rate ε [cm^{2}s^{-3}] of the water are determined from the paddle rotation rate via two calibrations. Equation

$$x = 0.017\omega + 0.0615 \quad \text{(B2)}$$

gives the relationship between x, gypsum dissolution rate in [g h^{-1}] as a proxy for turbulence intensity, and ω, the rotation rate in [RPM], as reconstructed from Petersen et al. (2009) who empirically derived this relationship for pelagic-benthic chambers of various dimension and construction. The second calibration empirically derived by Porter et al. (2000) using an acoustic Doppler velocity profiler (ADVP) relates U_{RMS} to gypsum dissolution rate in a fluctuating flow environment with the Eq. (B3),

$$U_{\mathrm{RMS}} = 15.6x - 0.8 \quad \text{(B3)}$$

where x is the dissolution rate [g h^{-1}] and U_{RMS} is in [cm s^{-1}]. Solving Eqs. (B2) and (B3) for x, the relationship between rotation rate and turbulence intensity is produced as shown in Eq. (B4):

$$U_{\mathrm{RMS}} = 0.2496\omega + 0.292\ . \quad \text{(B4)}$$

From U_{RMS} the turbulent dissipation rate can be estimated using Eq. (B5),

$$\varepsilon = \frac{U_{\mathrm{RMS}}^3}{l} \quad \text{(B5)}$$

where l is the integral length scale (largest eddy size) (Sanford, 1997; Petersen et al., 2009). In another investigation using the same MEERC benthic/pelagic type C tank, Porter et al. (2000) measured average volume weighted turbulence dissipation rates of 0.08 cm^2 s^{-3} and average volume weighted U_{RMS} of 1.08 cm s^{-1}, from which a bulk estimate of the length scale can be approximated to l = 15.7464 cm. In culmination, the paddle rotation rate can be used to approximate ε within the mixing chamber (Fig. 4 and Table 2), and also to compare the turbulence in the chamber with turbulence in the surface layer of the ocean under various wind conditions.

Acknowledgements. Thank you to Diksha Bista, Tapiwa Mubeda, Adriana Trutzenberg, Julian Thuemer, Ann Zellers, Maik Dressel and Michael Hofbauer for their support. This work was funded through the European Community's Seventh framework programme (FP7/2007-2013) under the HERMIONE project (Grant agreement No. 226354).

References

Andrady, A. L.: Microplastics in the marine environment, Elsevier Ltd., Mar. Pollut. Bull., 62, 1596–605, doi:10.1016/j.marpolbul.2011.05.030, 2011.

Barnes, D. K., Galgani, F., Thompson, R. C., and Barlaz, M.: Accumulation and fragmentation of plastic debris in global environments, Philos. T. R. Soc. Lond. B, 364, 1985–1998, doi:10.1098/rstb.2008.0205, 2009.

Browne, M., Galloway, T. S., and Thompson, R. C.: Spatial patterns of plastic debris along Estuarine shorelines, Environ. Sci. Technol., 44, 3404–3409, doi:10.1021/es903784e, 2010.
Claessens, M., Meester, S. D., Landuyt, L. V., Clerck, K. D., and Janssen, C. R.: Occurrence and distribution of microplastics in marine sediments along the Belgian coast, Elsevier Ltd., Mar. Pollut. Bull., 62, 2199–2204, doi:10.1016/j.marpolbul.2011.06.030, 2012.
Cole, M., Lindeque, P., Halsband, C., and Galloway, T. S.: Microplastics as contaminants in the marine environment: A review, Mar. Pollut. Bull., 62, 2588–2597, Elsevier Ltd., doi:10.1016/j.marpolbul.2011.09.025, 2011.
Costa, M. F., Ivar do Sul, J., Silva-Cavalcanti, J. S., Araújo, M. C. B., Spengler, A., and Tourinho, P. S.: On the importance of size of plastic fragments and pellets on the strandline: a snapshot of a Brazilian beach, Environ. Monit. Assess., 168, 299–304, doi:10.1007/s10661-009-1113-4, 2010.
Costa, M. F., Silva-Cavalcanti, J. S., and Barletta, M.: Plastics buried in the inter-tidal plain of an estuarine system, J. Coastal Res., SI 64 (Proceedings of the 11th International Coastal Symposium), 339–343, Szczecin, Poland, ISSN: 0749-0208, 2011.
Crawford, S. and Sanford, L.: Boundary-shear velocities and fluxes in the MEERC experimental ecosystems, Mar. Ecol.-Prog. Ser., 210, 1–12, doi:10.3354/meps210001, 2001.
Derraik, J. G. B.: The pollution of the marine environment by plastic debris: a review, Mar. Pollut. Bull., 44, 842–852, 2002.
Doyle, M. J., Watson, W., Bowlin, N. M., and Sheavly, S. B.: Plastic particles in coastal pelagic ecosystems of the Northeast Pacific ocean, Elsevier Ltd., Mar. Environ. Res., 71, 41–52, doi:10.1016/j.marenvres.2010.10.001, 2011.
Ferreira, T. and Rasband, W.: ImageJ User Guide IJ 1.45m, 179 pp., 2011.
Galgani, F., Souplet, A., and Cadiou, Y.: Accumulation of debris on the deep sea floor off the French Mediterranean coast, Mar. Ecol.-Prog. Ser., 142, 225–234, 1996.
Galgani, F., Leauteà, J. P., Moguedetà, P., Souplet, A., Verin, Y., Carpentier, A., and Vilar, J.: Litter on the Sea Floor Along European Coasts, Mar. Pollut. Bull., 40, 516–527, doi:10.1016/S0025-326X(99)00234-9, 2000.
Kukulka, T., Proskurowski, G., Morét-Ferguson, S., Meyer, D. W., and Law, K. L.: The effect of wind mixing on the vertical distribution of buoyant plastic debris, Geophys. Res. Lett., 39, 1–6, doi:10.1029/2012GL051116, 2012.

Lattin, G. L., Moore, C. J., Zellers, A. F., Moore, S. L., and Weisberg, S. B.: A comparison of neustonic plastic and zooplankton at different depths near the southern California shore, Mar. Pollut. Bull., 49, 291–304, doi:10.1016/j.marpolbul.2004.01.020, 2004.
Law, K. L., Morét-Ferguson, S., Maximenko, N., Proskurowski, G., Peacock, E. E., Hafner, J., and Reddy, C. M.: Plastic accumulation in the North Atlantic subtropical gyre, Science, 329, 1185–1188 , doi:10.1126/science.1192321, 2010.
MacKenzie, B. and Leggett, W.: Wind-based models for estimating the dissipation rates of turbulent energy in aquatic environments: empirical comparisons, Mar. Ecol.-Prog. Ser., 94, 207–216, doi:10.3354/meps094207, 1993.
Martinez, E., Maamaatuaiahutapu, K., and Taillandier, V.: Floating marine debris surface drift: convergence and accumulation toward the South Pacific subtropical gyre, Elsevier Ltd., Mar. Pollut. Bull., 58, 1347–1355, doi:10.1016/j.marpolbul.2009.04.022, 2009.
McDermid, K. J. and McMullen, T. L.: Quantitative analysis of small-plastic debris on beaches in the Hawaiian archipelago, Mar. Pollut. Bull., 48, 790–794, doi:10.1016/j.marpolbul.2003.10.017, 2004.
Moore, C. J., Moore, S. L., Leecasterà, M. K., and Weisbergà, S. B.: A Comparison of Plastic and Plankton in the North Pacific Central Gyre, Mar. Pollut. Bull., 42, 1297–1300, 2001.
Moore, C. J., Lattin, G. L., and Zellers, A. F.: Quantity and type of plastic debris flowing from two urban rivers to coastal waters and beaches of Southern California, Journal of Integrated Coastal Zone Management, 11, 65–73, 2011.
Morét-Ferguson, S., Law, K. L., Proskurowski, G., Murphy, E. K., Peacock, E. E., and Reddy, C. M.: The size, mass, and composition of plastic debris in the western North Atlantic Ocean, Mar. Pollut. Bull., 60, 1873–1878, 2010.
Mordecai, G., Tyler, P., Masson, D. G., and Huvenne, V. I.: Litter in submarine canyons off the west coast of Portugal, Elsevier Ltd., Deep-Sea Res. Part II, 58, 2489–2496, doi:10.1016/j.dsr2.2011.08.009, 2011.
Pabortsava, K., Purser, A., Wagner, H., and Thomsen, L.: The influence of drill cuttings on physical characteristics of phytodetritus, Mar. Pollut. Bull., 62, 2170–80, doi:10.1016/j.marpolbul.2011.07.002, 2011.
Pando, S., de Jesus Mendes, P., Thomsen, L., Coelho, H., and Neves, R.: A Modeling Approach to the Study of Organo-mineral aggregates in the Nazaré Canyon, EU-HERMIONE, Jacobs University Bremen, 2011.

Petersen, J., Kennedy, V., Dennison, W., and Kemp, W. (Eds.): Enclosed Experimental Ecosystems and Scale: Tools for Understanding and Managing Coastal Ecosystems, Springer Science and Business Media, New York, NY, doi:10.1007/978-0-387-76767-3, http://books.google.de, (last access: May 2012), 2009.

Porter, E. T., Sanford, L. P., and Suttles, S. E.: Gypsum dissolution is not a universal integrator of "water motion", American Society of Limnology and Oceanography, 45, 145–158, 2000.

Porter, E., Mason, R., and Sanford, L.: Effect of tidal resuspension on benthic–pelagic coupling in an experimental ecosystem study, Mar. Ecol.-Prog. Ser., 413, 33–53, doi:10.3354/meps08709, 2010.

Proskurowski, G., Law, K. L., Morét-Ferguson, S., and Reddy, C.: Abstract: The Impact of Wind Stress on the Concentration of Plastic Debris in the Open Ocean, Presented at the Ocean Sciences Meeting, Portland, OR, 2010.

Rasband, W. S.: ImageJ, US National Institutes of Health, Bethesda, Maryland, USA, http://imagej.nih.gov/ij/, 1997–2012.

Ryan, P. G., Moore, C. J., van Franeker, J., and Moloney, C. L.: Monitoring the abundance of plastic debris in the marine environment, Philos. T. R. Soc. Lond. B., 364, 1999–2012, doi:10.1098/rstb.2008.0207, 2009.

Sanford, L. P.: Turbulent mixing in experimental ecosystem studies, Mar. Ecol.-Prog. Ser., 161, 265–293, 1997.

Stiansen, J. and Sundby, S.: Improved methods for generating and estimating turbulence in tanks suitable for fish larvae experiments, Sci. Mar., 65, 151–167, 2001.

Thompson, R., Olsen, Y., Mitchell, R., Davis, A., Rowland, S., John, A., McGonigle, D., and Russell, A.: Lost at sea: where is all the plastic?, Science, 304, 5672, doi:10.1126/science.1094559, 2004.

Thomsen, L., VanWeering, T., and Gust, G.: Processes in the benthic boundary layer at the Iberian continental margin and their implication for carbon mineralization, Prog. Oceanogr., 52, 315–329, 2002.

Tolhurst, T. J., Black, K. S., Paterson, D. M., Mitchener, H. J., Termaat, G. R., and Shayler, S.: A comparison and measurement standardisation of four in situ devices for determining the erosion shear stress of intertidal sediments, Cont. Shelf Res., 20, 1397–1418, doi:10.1016/S0278-4343(00)00029-7, 2000.

Turner, A. and Holmes, L.: Occurrence, distribution and characteristics of beached plastic production pellets on the island of Malta (central Mediterranean), Mar. Pollut. Bull., 62, 377–381, Elsevier Ltd., doi:10.1016/j.marpolbul.2010.09.027, 2011.

USEPA: Plastic pellets in the aquatic environment: Sources and recommendations, EPA Oceans and Coastal Protection Division Report 842-B-92-010, Washington, DC, 1992.

Table 1. Resuspension steps of shear velocity for bedload transport, resuspension and deposition within erosion microcosm containing saltwater of density $\rho = 1026.20\,\mathrm{kg\,m^{-3}}$.

Step	U^* [cm s^{-1}]	τ [N m^{-2}]
1	0.37	1.4×10^{-2}
2	0.58	3.5×10^{-2}
3	0.76	5.9×10^{-2}
4	0.92	8.7×10^{-2}
5	1.07	0.12
6	1.21	0.15
7	1.33	0.18
6–	1.21	0.15
5–	1.07	0.12
4–	0.92	8.7×10^{-2}
3–	0.76	5.9×10^{-2}
2–	0.58	3.5×10^{-2}
1–	0.37	1.4×10^{-2}

Table 2. This table shows the turbulence intensities (U_{RMS}) and turbulence dissipation rates (ε) generated as a function of the rotation speed (RPM) of the paddles in a 1 m^3 MEERC pelagic/benthic water column simulation tank. The turbulent dissipation rates are given in two units to allow for simpler comparison to values found in natural systems (usually given in [W m^{-3}]). Correlated wind speeds, W, generating ε values at a depth of 0.5 m are calculated from Eq. (2), and allow for comparison between the laboratory turbulence experiments and field data.

Step	RPM [s^{-1}]	U_{RMS} [cm s^{-1}]	ε [cm^2 s^{-3}]	ε [W m^{-3}]	W [m s^{-1}]
0	0	0.29	1.58×10^{-3}	1.58×10^{-4}	2.39
1	3	1.04	7.16×10^{-2}	7.16×10^{-3}	8.50
2	6	1.79	0.36	3.64×10^{-2}	14.62
3	9	2.54	1.04	0.10	20.48
4	12	3.29	2.26	0.23	27.03
5	15	4.04	4.18	0.42	33.04
6	18	4.79	6.96	0.70	39.18
7	21	5.53	10.76	1.08	45.27
8	24	6.28	15.75	1.58	51.39
9	27	7.03	22.08	2.21	57.48

Table 3. Number of pieces (n), mean and standard deviation of area, Feret's diameter or length (indicated with *) and minimum Feret's diameter in mm for each collection site and debris type.

	n	Area [mm^2] (Mean ± SD)	Feret's Diameter/ Length* [mm] (Mean ± SD)	Minimum Feret's Diameter [mm] (Mean ± SD)
LA Beach (area not known; sandy) n = 1116				
HD Black pellet	133	11.521 ± 1.691	4.709 ± 0.333	3.451 ± 0.285
HD Opaque Pellet	148	11.052 ± 2.207	4.417 ± 0.474	3.347 ± 0.362
HD Transparent Pellet	290	13.739 ± 2.113	5.089 ± 0.358	3.76 ± 0.342
LD Pellet	483	15.675 ± 2.554	4.983 ± 0.406	4.267 ± 0.338
HD Fragment	17	51.703 ± 26.097	12.011 ± 5.252	6.356 ± 2.078
LD Fragment	45	71.958 ± 33.54	13.429 ± 4.136	8.059 ± 2.602
Elbe River Strandline – Site 1 (~ 100 dm^3 flotsam) n = 714				
Pellet	69	11.497 ± 7.904	3.958 ± 1.798	3.152 ± 1.550
Fragment Large	18	200.949 ± 191.79	37.733 ± 25.075	10.563 ± 7.751
Fragment Medium	41	48.974 ± 36.645	15.882 ± 7.103	5.211 ± 2.875
Fragment Small	337	10.659 ± 11.828	5.291 ± 2.725	2.759 ± 1.392
Foam	12	66.902 ± 108.67	9.991 ± 7.442	6.718 ± 4.951
Film Large	21	345.209 ± 355.956	35.318 ± 28.086	14.564 ± 6.734
Film Small	134	38.16 ± 37.4	11.519 ± 7.046	4.965 ± 2.903
Filament	82	–	19.713 ± 23.502*	–
Elbe River Strandline – Site 2 (~ 100 dm^3 flotsam) n = 495				
Pellet	50	14.285 ± 3.952	4.596 ± 0.874	4.007 ± 0.508
Fragment	20	137.899 ± 164.584	22.192 ± 20.672	8.113 ± 6.888
Foam	422	91.779 ± 230.245	11.335 ± 9.548	7.506 ± 5.501
Film	1	741.434	54.016	20.584
Filament	2	–	15.003 ± 3.865*	–
Weser River Strandline – Site 1 (~ 100 dm^3 flotsam) n = 67				
Pellet	13	15.073 ± 6.128	4.73 ± 1.262	3.927 ± 1.043
Fragment	26	34.113 ± 77.528	10.138 ± 15.202	3.51 ± 1.99
Foam	19	40.265 ± 40.877	8.477 ± 4.982	5.754 ± 3.124
Filament	9	–	38.712 ± 49.93*	–
Weser River Strandline – Site 2 (~ 100 dm^3 flotsam) n = 16				
Pellet	5	19.519 ± 9.611	5.789 ± 1.443	4.386 ± 1.051
Fragment	9	15.116 ± 10.370	7.063 ± 4.571	3.087 ± 1.289
Foam	2	14.389 ± 0.742	5.696 ± 0.512	4.039 ± 0.103

Table 4. The mean densities of the LA Beach subsamples. Standard deviations indicate differences between measurement replicates.

Subsample	Density [g cm^{-3}] (Mean ± SD)
HD Black pellet	1.06 ± 0.04
HD Opaque pellet	1.07 ± 0.08
HD Transparent pellet	1.13 ± 0.01
LD pellet	0.71 ± 0.04

Table 5. The mean and median settling speed of the high density subsamples from the LA Beach sample averaged from ∼50 pellets dropped through saltwater column $\rho = 1026.69\,\mathrm{kg\,m^{-3}}$.

	Settling Velocity [$\mathrm{mm\,s^{-1}}$] (Mean ± SD)	Median [$\mathrm{mm\,s^{-1}}$]
HD Black pellet	28.20 ± 3.19	28.74
HD Opaque pellet	23.07 ± 5.69	23.12
HD Transparent pellet	41.27 ± 21.44	39.58

Table 6. Bedload, critical and depositional velocities, U^* [$\mathrm{m\,s^{-1}}$] and shear stresses, τ [$\mathrm{N\,m^{-2}}$] for high-density pellets averaged from repetitive experiments in saltwater $\rho = 1026.69\,\mathrm{kg\,m^{-3}}$, using a 20 cm diameter resuspension chamber. Values are approximated and replicate averaged.

	Bedload Shear		Critical Shear		Depositional Shear	
	U^*_b	τ_b	U^*_{cr}	τ_{cr}	U^*_d	τ_d
HD Black Pellets	4.9×10^{-3}	2.5×10^{-2}	1.1×10^{-2}	0.14	9.2×10^{-3}	8.7×10^{-2}
HD Opaque/Transparent Pellets	$> 1.3 \times 10^{-2}$	> 0.18	$\gg 1.3 \times 10^{-2}$	$\gg 0.18$	6.7×10^{-3}	4.6×10^{-2}

Table 7. HD black pellets and benthic boundary layer aggregates (Thomsen et al., 2002) transport properties are compared.

	d_{50} [µm]	ρ [g cm^{-3}]	Settling Velocity [mm s^{-1}]	τ_{cr} [N m^{-2}]
HD Black Pellet	4700	1.06	28.20	0.14
BBL Aggregate (Thomsen et al., 2002)	4000	1.03	4.77	0.026

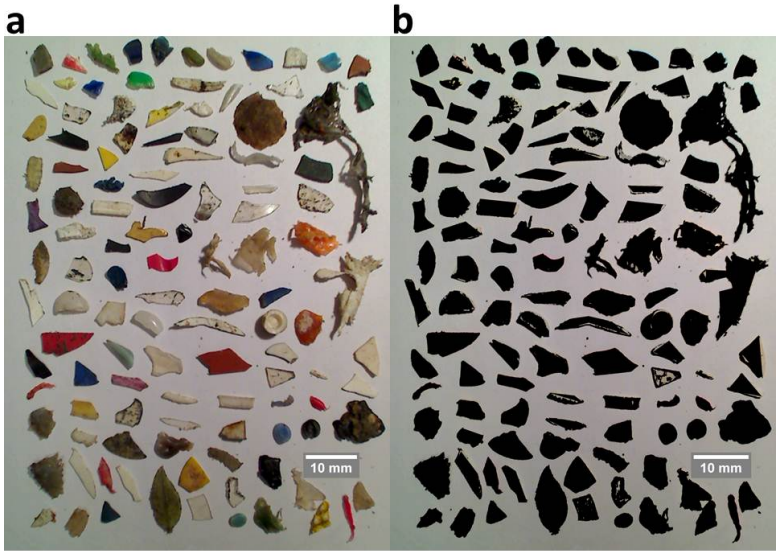

Fig. 1. Photographed subsample of fragments from Elbe Site 1 in **(a)** with color threshold applied in **(b)** for use of the 'Measure Particles' tool of the *ImageJ* (Rasband, 1997–2012) image analysis software application.

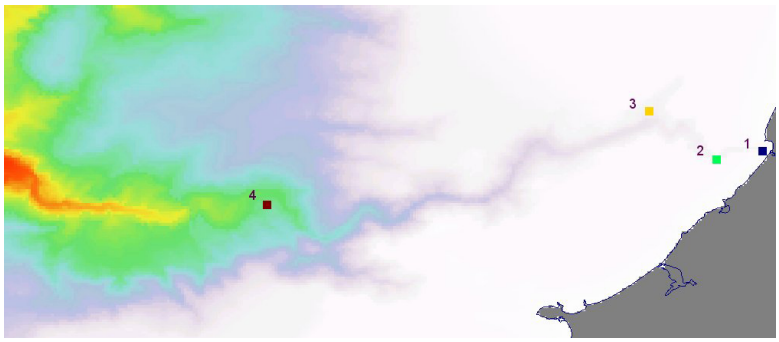

Fig. 2. The locations of the monitor boxes in the MOHID model simulation of the dispersal of plastic preproduction pellets in the Nazaré Canyon off the coast of Portugal. Boxes lie along the canyon axis and are 0.5 m^3 in volume, each initially containing ~ 2000 pellets. Canyon topography and depth is depicted in the color scale; purple < 1000 m, blue < 2000 m, green < 3000 m, yellow < 4000 m, red < 5000 m.

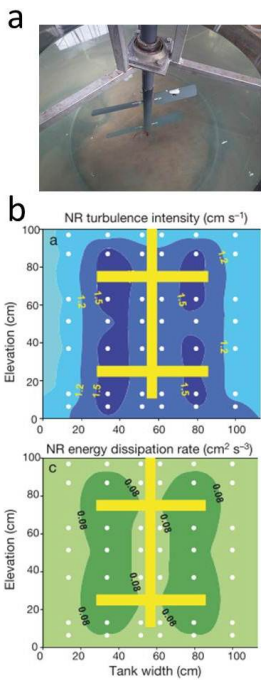

Fig. 3. (a) The 1 m^3 cylindrical MEERC water column simulation tank with two sets of inclined paddles rotated around a vertical axis generates turbulence intensities similar to those found in the surface and mixed layer of the upper ocean. **(b)** Upper plot shows turbulence intensity cross-section and lower plot shows energy dissipation rates in 1 m^3 water column simulation tank used for the imitation of turbulence in an estuary. White dots are measurement locations (See Appendix B) and the yellow area depicts the stirring rod and paddles (Porter et al., 2010).

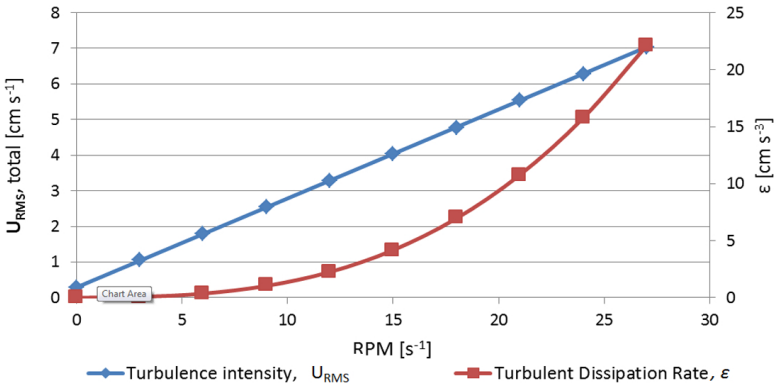

Fig. 4. The turbulence intensities (U_{RMS}) and turbulence dissipation rates (ε) generated as a function of the paddle rotation speed (RPM) within a 1 m^3 pelagic-benthic water column simulation tank.

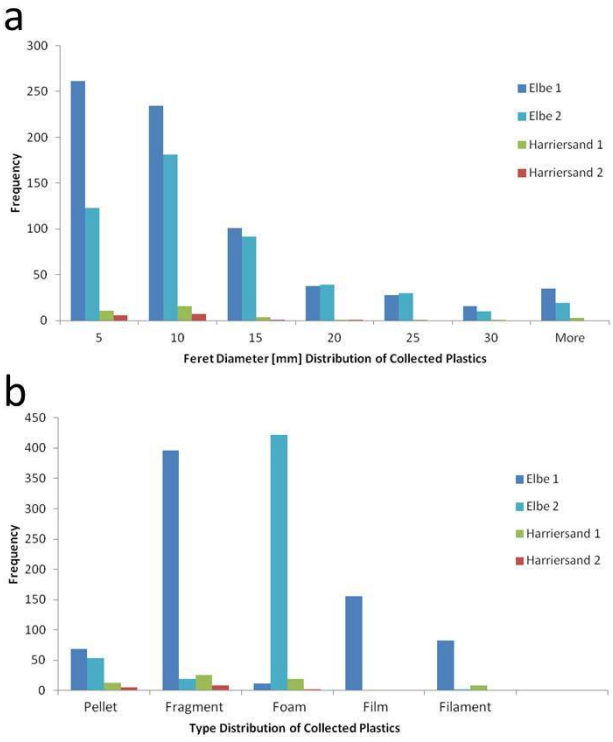

Fig. 5. Plastic samples from four collection sites (Elbe and Weser River strandlines) sorted by **(a)** size (according to Feret's diameter or length for filaments) in bins of 5 mm up to 30 mm and **(b)** type (pre-production pellet, fragment, foam, film and filament) and plotted against frequency.

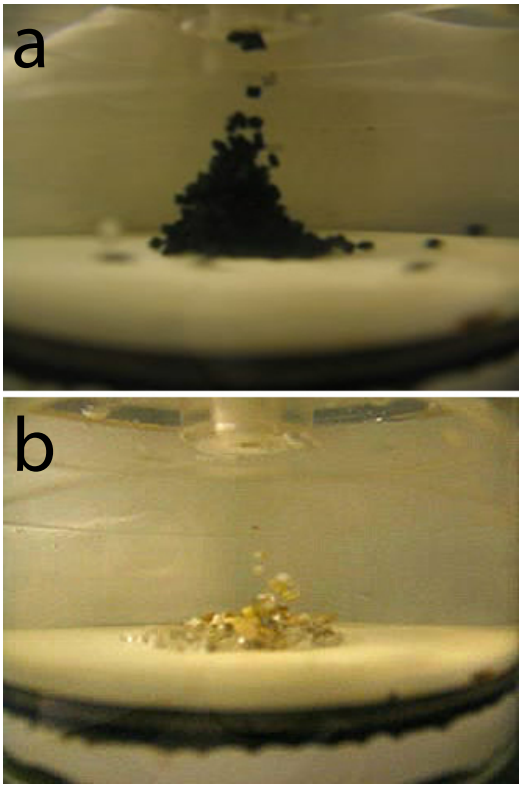

Fig. 6. (a) HD black pellets and **(b)** HD opaque/transparent pellets in erosion chamber each during step 7 ($\tau = 0.18\,\mathrm{N\,m^{-2}}$) of replicate run 4. Still image extracted from video recording.

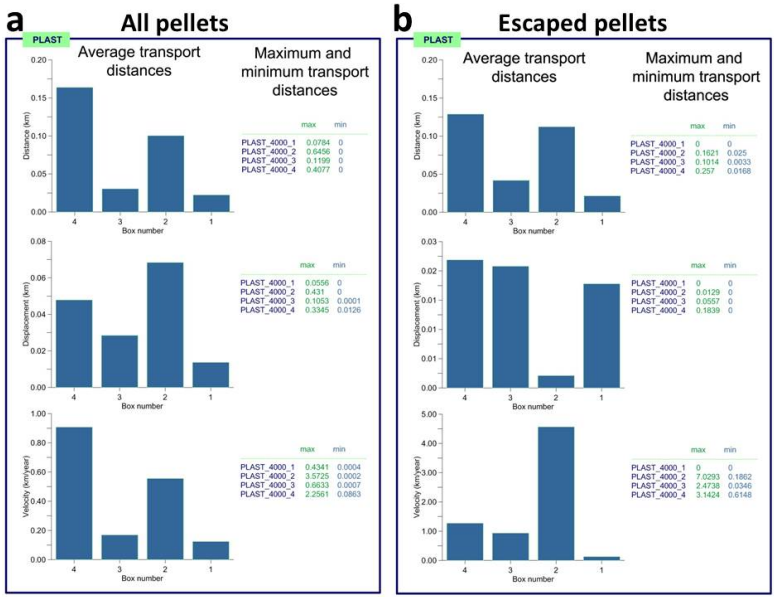

Fig. 7. Nazaré canyon model results showing average displacement [km], distance [km] and velocity [km $\mathrm{yr^{-1}}$] of HD black pellets during the time period of 56 days in Spring 2009. Box number corresponds to monitor boxes along canyon axis. **(a)** shows averages for all 2004 pellets initially in each monitor box, while **(b)** shows the averages for only the particles which escaped the box; 1, 13, 53 and 39 pellets for Box 1 to Box 4, respectively. Minimum and maximum values for each monitor box are also shown.

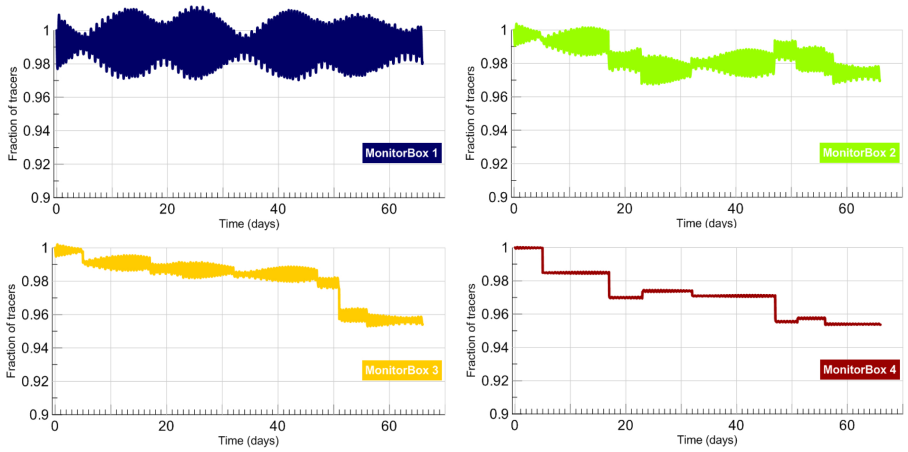

Fig. 8. The residence time of the HD black pellets in each box of the Nazaré Canyon is depicted here as the fraction of tracers (pellets) located inside the 0.5 m^3 monitor box over time (days) for the simulation period (56 days).

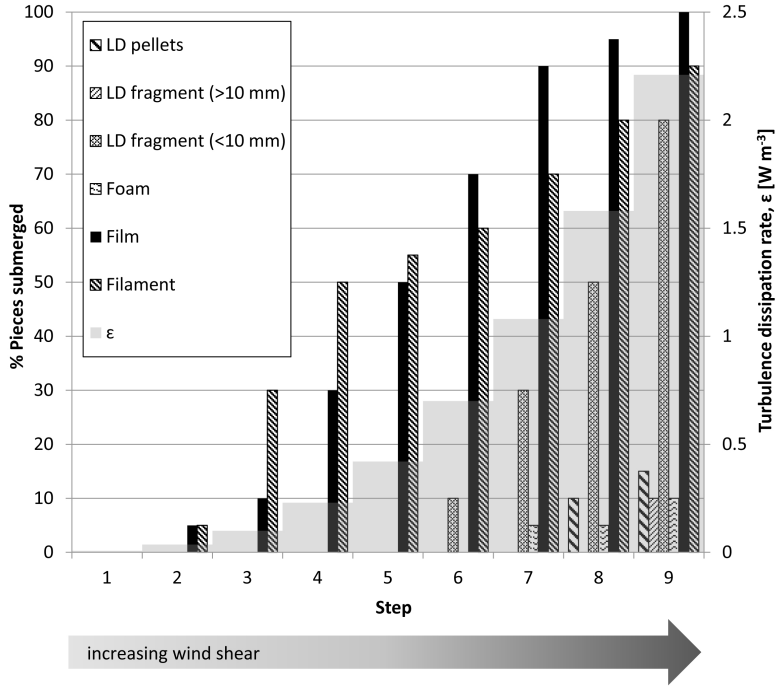

Fig. 9. Approximate percentages of microplastic pieces submerged and the corresponding turbulence dissipation rate [W m^{-3}] averaged for the entire volume of the MEERC benthic/pelagic tank filled with salt water of density $\rho = 1026.69\,kg\,m^{-3}$ at each step of increased paddle rotation rate of the turbulence assay.

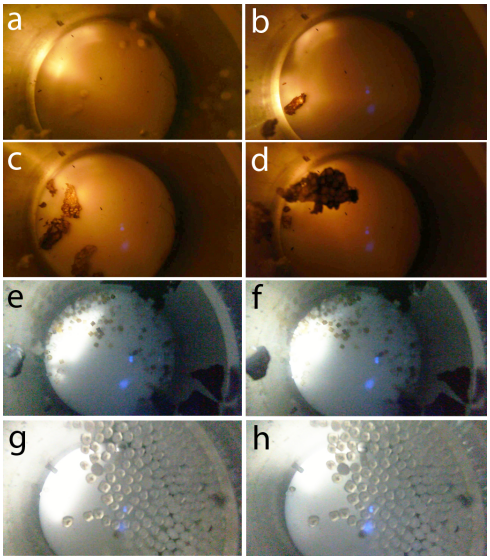

Fig. 10. Downward views inside the interior pressure chamber containing water of salinity 36 psu; still images were extracted from video recordings of camera inside pressure housing. **(a)** Foam subsample from Elbe site 2; pressure: 1 bar (white spheres are buoyant Styrofoam pieces), **(b)** 60 bar (one piece has lost buoyancy), **(c)** 170 bar (several large biofilmed Styrofoam pieces have lost buoyancy) and **(d)** 20 bar during pressure release (most pieces have regained buoyancy). Other pieces, which did not sink are not visible due to limited camera view. LD fragments, HD opaque pellets and HD transparent pellets inside the interior pressure chamber at **(e)** 1 bar pressure and **(f)** 200 bar. LD pellets at a pressure of **(g)** 1 bar and **(h)** 200 bar. No changes in vertical distribution were observed during the experiment runs for LD fragments, HD opaque pellets, HD transparent pellets or LD pellets.

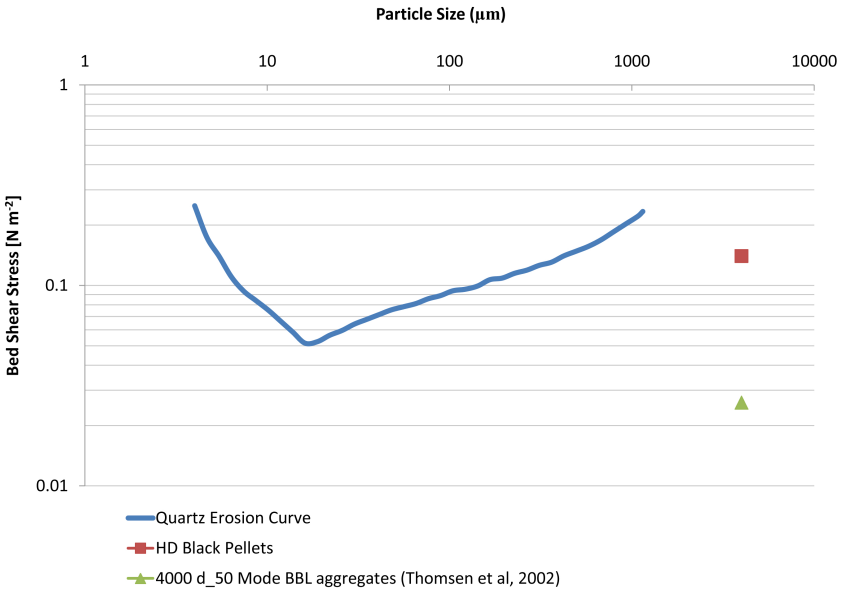

Fig. 11. The critical bed shear stress erosion curve for quartz relates particle (sediment) size to critical shear stress, τ_{cr}, and includes average diameter (d_{50}) 4 mm benthic boundary layer aggregate data point (Thomsen et al., 2002). The mean HD black pellet size ($d_{50} \sim 4$ mm) and τ_{cr} is plotted over the curve for comparison of aggregate and plastic erosional behavior.